J. Astrophys. Astr. (2020) 41:10
https://doi.org/10.1007/s12036-020-9627-9

Hα full line spectropolarimetry as diagnostics of chromospheric magnetic field

K. NAGARAJU[1,*], K. SANKARASUBRAMANIAN[2] and K. E. RANGARAJAN[1]

[1]Indian Institute of Astrophysics, Bengaluru 560 034, India.
[2]U R Rao Satellite Centre, Bengaluru 560 094, India.
*Corresponding author. E-mail: nagarajuk@iiap.res.in

MS received 19 September 2019; accepted 30 January 2020

Abstract. Analysis of spectropolarimetric observations of two circular sunspots located close to disk centre in Hα (6562.8 Å) and Fe I (6569.22 Å) is presented in this paper. The corresponding active region numbers are NOAA 10940 and NOAA 10941 referred to as AR1 and AR2, respectively. The vector magnetic field at the photosphere is derived through inversion of Stokes profiles of Fe I under Milne–Eddington atmospheric model. The chromospheric vector magnetic field is derived from Hα Stokes profiles under weak-field approximation. Azimuthally averaged magnetic field as a function of radial distance from the centre of sunspot at the photosphere and chromosphere are studied. At the photosphere, the radial variation shows a well known behaviour that the total field and the line-of-sight (LOS) component monotonically decrease from centre to the edge of the sunspot and the transverse component initially increases, reaches a maximum close to half the sunspot radius and then decreases. LOS and the transverse components become equal close to half the sunspot radius consistent with the earlier findings. At the chromosphere, all the components of the magnetic field decrease with the sunspot radius. However, the LOS component decreases monotonically whereas the transverse component decreases monotonically up to about 0.6 times the sunspot radius after which it reaches a constant value. Azimuthally averaged magnetic field gradient from photosphere to chromosphere is also presented here.

Keywords. Sun:Magnetic field—Sun:Photosphere—Sun:Chromosphere.

1. Introduction

Magnetic field plays a crucial role of coupling different layers in the solar atmosphere from photosphere and below through chromosphere to corona and beyond. Hence simultaneous knowledge of magnetic field at different layers is important. Magnetic field measurements at the photosphere is relatively well established. There has been considerable progress in the recent past towards magnetic field measurements in the chromosphere (Lagg *et al.* 2017). The spectral lines at 10,830 Å due to He I and at 8542 Å due to Ca II have been the most widely used lines to measure the magnetic field in chromosphere. The He I line forms at the upper chromospheric layers. While it is an advantage for this line which forms over a very narrow height range so that Milne–Eddington atmosphere-based inversions can be used to infer magnetic field and other atmospheric parameters, it is a limitation of this line to probe only a small range of atmospheric layers. Further, the line formation strongly depends on the coronal ultra-violet radiation emission (Andretta & Jones 1997). On the other hand Ca II forms all the way from photosphere (line wings) to middle of the chromosphere (line core; Uitenbroek 2006). However, in the flare regions this line may sample only the deeper layers of the solar atmosphere (Kerr *et al.* 2016; Kuridze *et al.* 2018). Due to intense heating Ca II atoms get ionized to Ca III (Kerr *et al.* 2016). Where as Hα is ubiquitous in the chromosphere which can probe wide range of chromospheric dynamics (Rutten 2008).

Hα is one of the most widely used spectral lines to study the solar chromosphere, mostly through the images recorded in and around the line core (Rutten 2007). However, the magnetic field measurements using this line are sparse. Simultaneous magnetic field measurements through spectropolarimetric observations in Hα and Fe I line at 6302.5 Å were reported by Abdussamatov (1971). Using these measurements field gradient was also estimated. Line-of-sight (LOS) magnetic

Published online: 24 March 2020

field derived using Hα spectropolarimetry have been reported by Balasubramaniam *et al.* (2004), Hanaoka (2005) and Nagaraju *et al.* (2008a) have compared the measurements with the simultaneous photospheric magnetic field measurements. The sunspot observed by Balasubramaniam *et al.* (2004) was a flaring active region. It was noted that Stokes V changes its sign when the line goes into the emission showing the consistency in the response of Hα line to change in physical conditions. Apart from observing active regions, Hα was also used in diagnosing prominence magnetic and electric field (López Ariste *et al.* 2005).

One of the reasons why Hα has not been a preferred line to probe the chromospheric magnetic field is because the observations are notoriously difficult to interpret. For e.g., a theoretical study by Socas-Navarro and Uitenbroek (2004) have reported an issue of ambiguity in sensitivity of Hα spectral features to different physical parameters at different heights. However, it has been shown by Leenaarts *et al.* (2012) through radiation–magneto-hydrodynamic simulations and 3D non-local thermodynamic equilibrium radiative transfer calculations that the ambiguity is due to 1D radiative transfer effects and emphasized that 3D radiative transfer calculations are essential in modelling the Hα line formation. In this study, it was shown that Hα is a good chromospheric magnetic field diagnostic. This finding was further supported by a recent work by Bjørgen *et al.* (2019). This has motivated us to re-look at some of our earlier Hα spectropolarimetric observations from Kodaikanal tower tunnel telescope (KTT).

In the present study, we present here about the analysis of Hα full line spectropolarimetric data above two sunspots located close to disk centre to understand the chromospheric magnetic field structure in conjunction with simultaneous photospheric magnetic field measurements. The observations presented in this study are of low spatial resolution ($\approx 5''$). Hence, the global properties of sunspot magnetic field simultaneously at the photosphere and chromosphere are presented here.

2. Observations, data reduction and analysis

Spectropolarimetric observations were carried out using a dual-beam polarimeter at KTT (Nagaraju *et al.* 2007). The KTT has a three mirror coelostat system which, during observations, constantly feeds the sunlight to the 38 cm doublet lens which images the sun at its focal plane with a focal length of 36 m. The plate scale at the focal plane is $5.''5$/mm. The telescope is equipped with a high-resolution Littrow mount spectrograph (see Bappu 1967 for more details) with the resolving power of $\approx$ 240,000 in the second-order diffraction spectrum. The details on the performance of this polarimeter and the spectrograph are discussed in Nagaraju *et al.* (2008b). The wavelength region of the observations includes the magnetically sensitive lines, Hα (6562.8 Å) and Fe I (6569.22 Å) with effective Landé g-factor of 1.048 (Casini & Landi Degl'Innocenti 1994) and 1.4 (Kobanov *et al.* 2003), respectively.

The spectropolarimetric data of active regions AR1 and AR2 presented here were obtained on 1 and 4 February 2007, respectively. The heliographic co-ordinates of AR1 during the observations were 4° south and 10.5° west and for AR2 they were 7° south and 5.5° east. Scanning of the region-of-interest (ROI) was done by moving the Sun's image in the east-west direction in steps of $\approx 2''$. For each slit position, the modulated intensities were recorded by a charge-coupled device (CCD) detector. CCD used for observations was a 2 K × 2 K detector supplied by Andor company (Belfast, Northern Ireland) with 13.5 μ square pixel and the pixels were binned 2 × 2 during the observations. With this arrangement, the spatial sampling along the slit is $0.''142$/pixel and the spectral sampling is 11.38 mÅ/pixel. For the purpose of simultaneous imaging and spectropolarimetry, a non-polarizing beam splitter (NPBS) was used to channel a part of the beam passing through the polarimeter in perpendicular direction. The images were recorded by another CCD using a wide band filter of band width 800 Å with the peak transmission centred at 6300 Å. The slit position on the image was identified by introducing an aperture in front of NPBS (see Nagaraju *et al.* 2008b for details). Sample images of AR1 (the left panel) and AR2 (the right panel) obtained using the broad-band filter are shown in Figure 1. The vertical line on AR1 represents one of the slit positions. The corresponding Stokes spectral images are shown in Figure 2. The seeing conditions during the observations of AR1 were better than that of AR2 which is clearly evident in these sample images.

The data were corrected for bias counts and gain table variation of the pixels. The correction for gain table variation is commonly known as flat fielding. For flat fielding, spectral images were recorded by moving the solar image randomly over the slit during exposure. The quiet sun region close to the disk centre, which is free from any visible activity was chosen for flat fielding. This provided uniform illumination of light along the slit. The master flat was obtained after removing the spectral features which was achieved by dividing individual spectral profile along the slit by a median spectral profile from a given spectral image

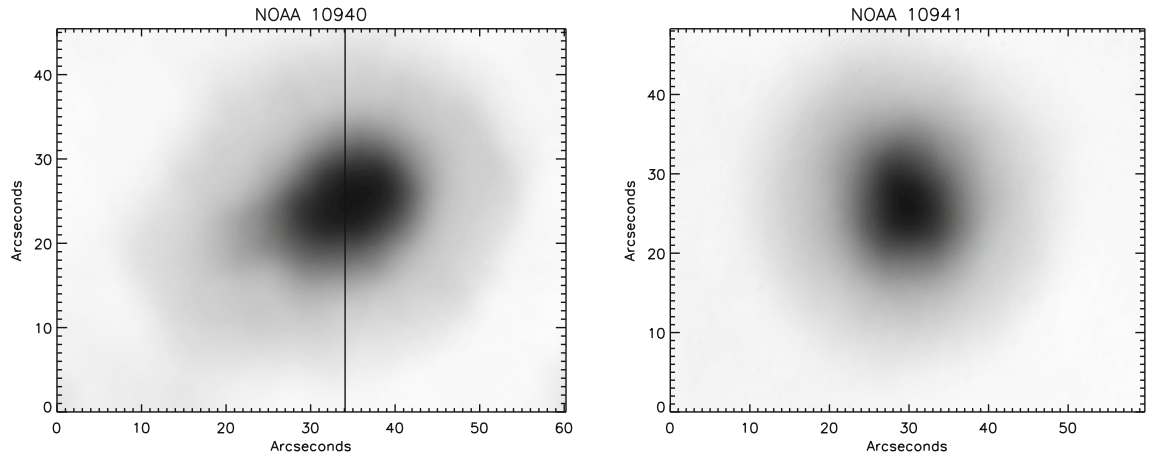

Figure 1. Wide band images of active regions analysed in this paper. The left panel image corresponds to AR1 and the left panel image corresponds to AR2. The direction of spatial scanning is from left to right. The origin of the coordinates in this figure is arbitrarily fixed.

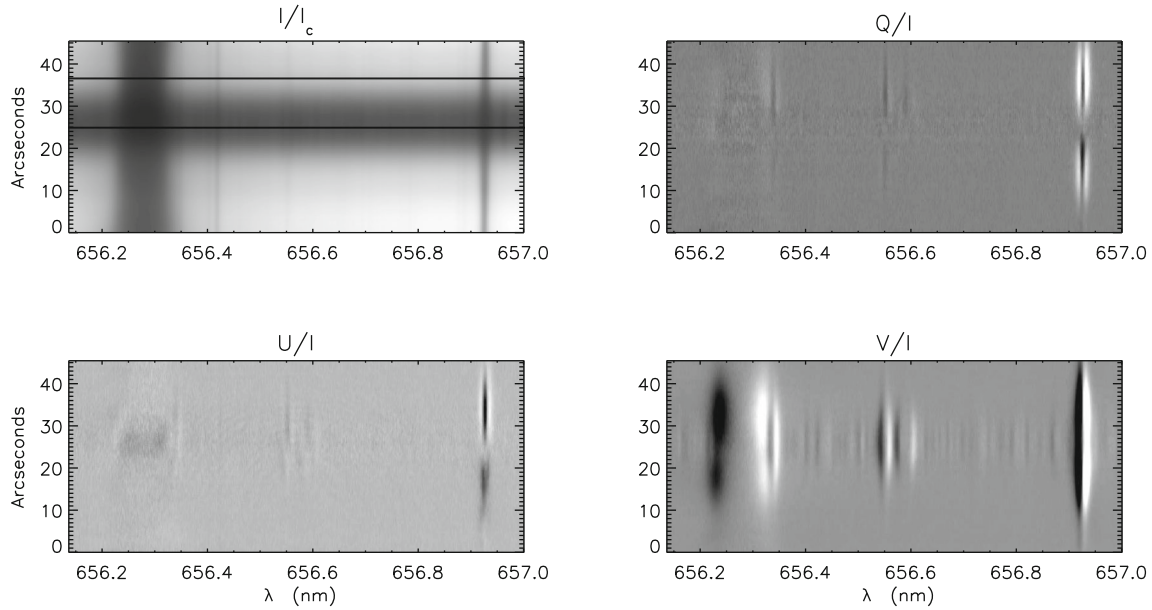

Figure 2. Sample Stokes spectral images for the slit position marked as vertical line on a context image of AR1 shown in Figure 1. The grey scale for Stokes I/I_c is between 0 and 1 and for Stokes Q, U and V it is between -0.05 and 0.05.

(see Nagaraju *et al.* 2008b for more details). The polarimeter response was corrected using the calibration data. The calibration unit consisting of a linear polarizer (Glan-Thomson prism) followed by a quarter waveplate used to generate known states of polarization. The calibration data were generated by positioning the fast axis of the calibration unit quarter waveplate every 15° from 0° to 180°. The process of deriving the response matrix is detailed in Nagaraju *et al.* (2007). The corrections for telescope induced cross-talks were done using a telescope model developed by Balasubramaniam *et al.* (1985) and Sankarasubramanian *et al.* (2000) and the residual cross-talks were corrected using a statistical method (Sanchez & Lites 1992; Schlichenmaier & Collados 2002). Further details on the reduction procedures of spectropolarimetric data obtained from KTT can be found in Nagaraju *et al.* (2008b).

The photospheric vector magnetic fields were obtained by inverting the Stokes profiles of Fe I line using Milne–Eddington based inversion codes. We have used advanced Stokes polarimeter (ASP) (Auer *et al.* 1977; Skumanich & Lites 1987; Lites & Skumanich 1990) and MELANIE (Socas-Navarro 2001) inversion codes for assuring the reliability of the inversion results. Both ASP and MELANIE perform

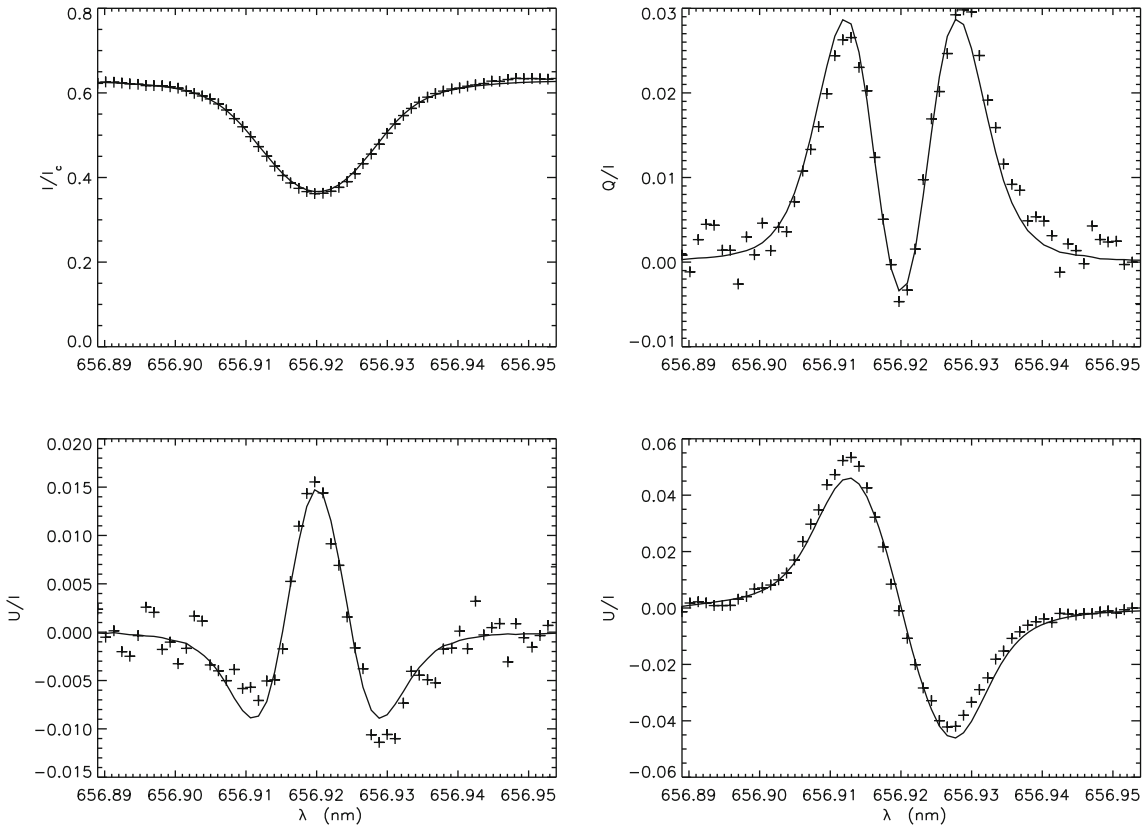

Figure 3. Plots of the observed (the plus symbols) and fitted (solid curves) Stokes profiles of Fe I line at 6569.2 Å corresponding to the spatial pixel marked by a horizontal line at 37″ on the Stokes I spectral image in Figure 2.

non-linear least-square fitting of the observed Stokes profiles under local thermodynamic equilibrium (LTE) conditions by assuming Milne–Eddington atmosphere. Milne–Eddington atmosphere is a simplified atmospheric model to model the spectral lines formed in the photosphere. It assumes that the source function is a linear function of the optical depth and the physical parameters such as velocity and magnetic fields are constant over the line formation depth. Inversion codes return magnetic field strength, inclination angle with respect to LOS, azimuth, line strength, damping parameter, LOS velocity, source function and its gradient with respect to optical depth, macroturbulence and fraction of stray light/fill factor of the non-magnetic component. The maximum error in estimating the magnetic field is ≈50 G, for the field inclination is about 5° and its azimuth is 6°. As an e.g., we have shown in Figure 3, the observed and fitted Stokes profiles corresponding to the spatial pixel indicated by the top horizontal line (at 37″) in Stokes I/I_c image as shown in Figure 2. The plus signs represent the observed and the solid curves represent the fitted Stokes profiles. The magnetic field measurements of AR1 carried out at Kodaikanal were compared with that of *Hinode*/SOT observations (see Nagaraju *et al.* 2008b for details). It was found that the comparison was one-to-one after the *Hinode*/SOT measurements were smoothed spatially by ≈ 5.12″.

The chromospheric vector magnetic fields were derived using weak field approximation (WFA) (Landi Degl'Innocenti & Landi Degl'Innocenti 1973; Jefferies & Mickey 1991; Landi Degl'Innocenti & Landolfi 2004) applied to the Stokes profiles of Hα. The parallel (B_z: along LOS) and the transverse (B_t: perpendicular to LOS) components of the field were calculated using the least square fit formulae (Martínez González & Bellot Rubio 2009; Centeno 2018)

$$B_z = -\frac{\sum_\lambda \frac{\partial I(\lambda)}{\partial \lambda} V(\lambda)}{C \sum_\lambda \left(\frac{\partial I(\lambda)}{\partial \lambda}\right)^2}, \quad (1)$$

$$B_t = \frac{2}{C}\left(\frac{\sum_\lambda \frac{L(\lambda)}{3}\left|\frac{1}{\lambda-\lambda_0}\right|\left|\frac{\partial I}{\partial \lambda}\right|}{\sum_\lambda \left|\frac{1}{\lambda-\lambda_0}\right|^2 \left|\frac{\partial I}{\partial \lambda}\right|^2}\right)^{1/2} \quad \text{for } \lambda = \lambda_w \quad (2)$$

where $L(\lambda) = \sqrt{Q(\lambda)^2 + U(\lambda)^2}$ and $C = 4.67 \times 10^{-13} g_{\rm eff} \lambda_0^2$ with λ_0, the line centre wavelength

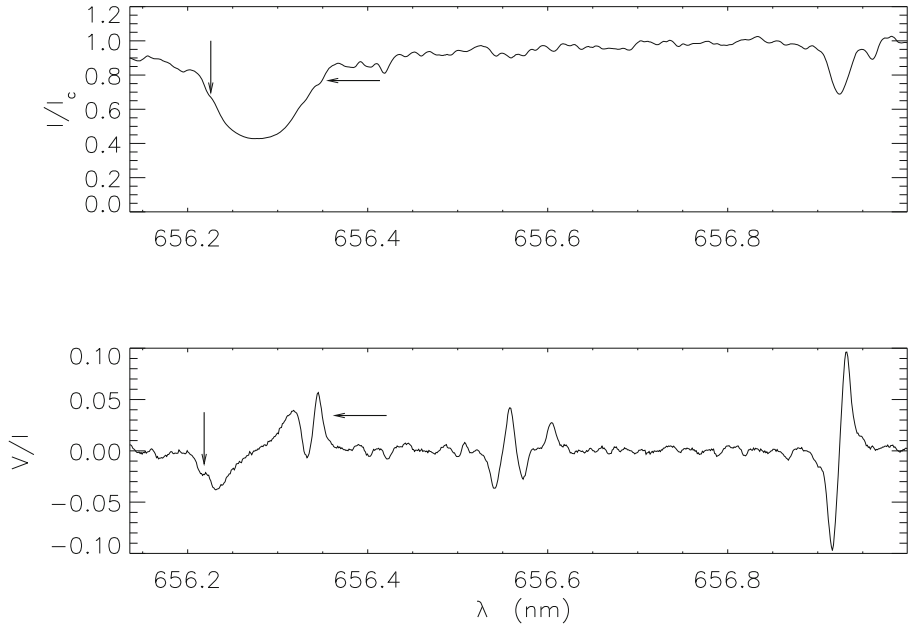

Figure 4. Sample Stokes I and V profiles close to sunspot centre. The horizontal arrows indicate the well-known blend due to Co I at 6563.4 Å and the vertical arrows indicate a blend of magnetically sensitive line at 656.224 nn in Hα. The corresponding spatial pixel is marked by a horizontal line at 25″ on the Stokes I spectral image in Figure 2.

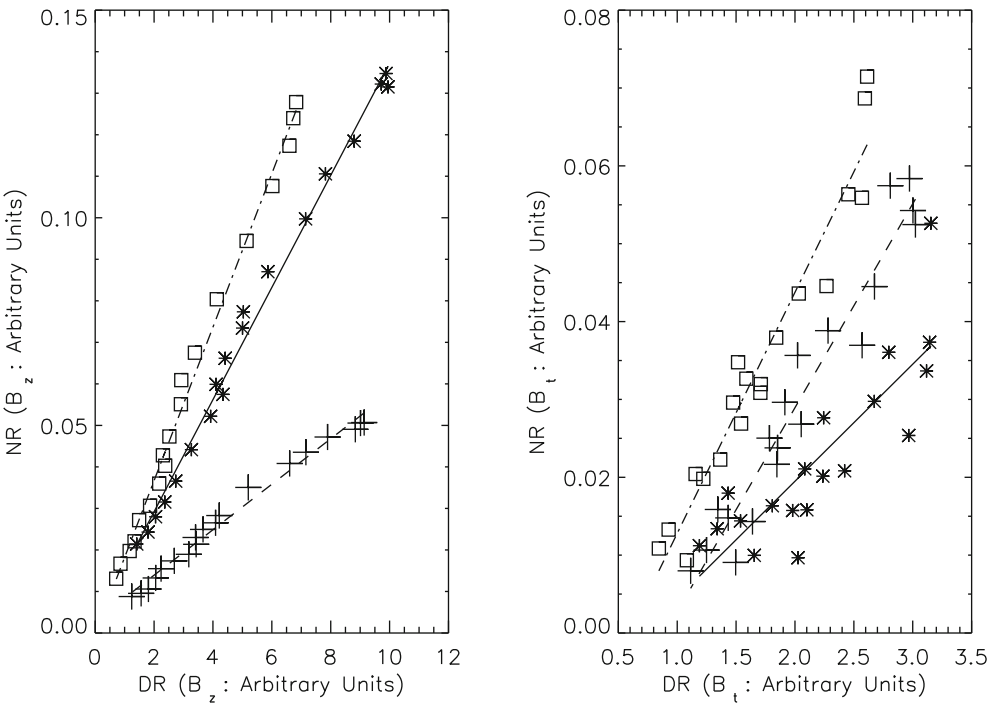

Figure 5. Plots to demonstrate the linear fit used for deriving the line-of-sight (LOS) (the left panel) and the transverse (the right panel) components of the magnetic field (cf. Equations (1) and (2)) under weak field approximation applied to Hα Stokes profiles. Three different symbols in these plots represent three different spatial pixels arbitrarily chosen from within AR1.

expressed in Å, $g_{\rm eff}$ the effective Landé g-factor of the atomic transition under consideration and λ_w is the wavelength point away from the line centre at which the magnetic field is calculated. The values were estimated at $\lambda_w = 6562.5$ Å (i.e. $-$ 300 mÅ away from the line centre) and for linear least-squares fit the wavelength

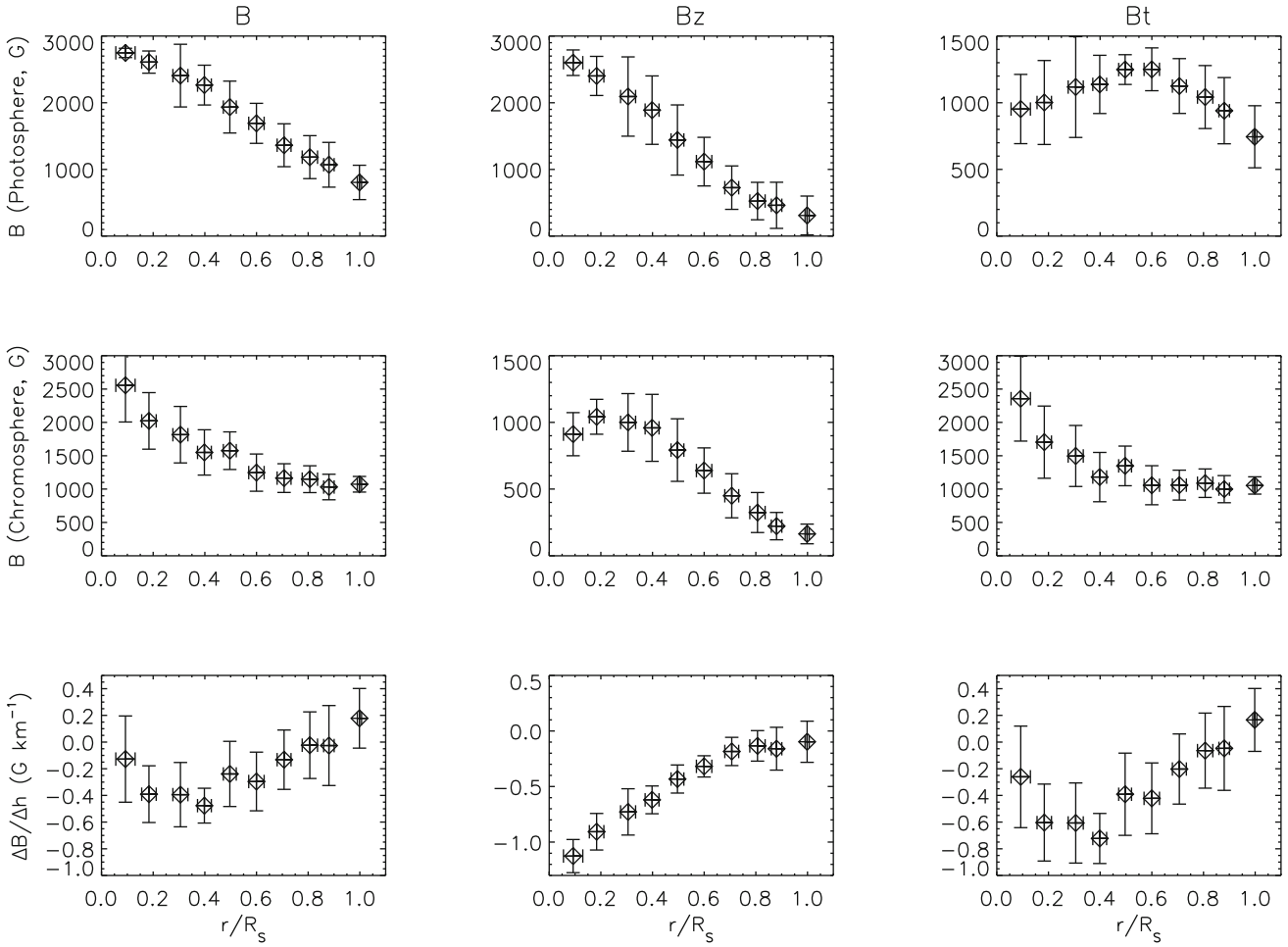

Figure 6. Plots of azimuthally averaged magnetic field parameters as a function of normalized radial distance (r/R_s) from the sunspot centre for AR1. The first and second row of panels show radial variation of magnetic field at the photosphere and chromosphere, respectively. The first, second and third column show the plots of B (total field strength), B_z (LOS component) and B_t (transverse component). The third row of panels correspond to the field gradient ($\Delta B/\Delta h$).

range considered was 100 mÅ around this wavelength. This particular wavelength was chosen as any wavelength point chosen in the red-wing either will be too close to the line centre where SNR is poorer or affected by the well known blend due to Co I at 6563.4 Å. The Co I is a magnetically sensitive line as indicated by the horizontal arrow on the Stokes I and V profiles shown in Figure 4. In the blue wing also there is a, not so well known, magnetically sensitive line blend at around 6562.24 Å, indicated by the vertical arrows in Figure 4, mostly seen in the umbral regions. At the moment it is not clear to which species this line belongs to. These observations emphasize the importance of full line spectropolarimetry in order to avoid any such artefacts in the field estimation.

The linear fit of the observed quantities used to derive LOS (Equation (1)) and transverse (Equation (2)) components of the magnetic field is shown in Figure 5. The left panel shows the plot of $\mathrm{NR}(B_z) = \frac{\partial I(\lambda)}{\partial \lambda} V(\lambda)$ vs. $\mathrm{DR}(B_z) = \left(\frac{\partial I(\lambda)}{\partial \lambda}\right)^2$, the quantities used for deriving the LOS component of the magnetic field (cf. Equation (1)). The right panel shows the plots of $\mathrm{NR}(B_t) = L(\lambda) \left| \frac{1}{\lambda - \lambda_0} \right| \left| \frac{\partial I}{\partial \lambda} \right|$ vs. $\mathrm{DR}(B_t) = \left| \frac{1}{\lambda - \lambda_0} \right|^2 \left| \frac{\partial I}{\partial \lambda} \right|^2$, the quantities used for deriving the transverse component of the magnetic field (cf. Equation (2)). The square, the star and the plus symbols correspond to different, arbitrarily chosen, spatial locations within the AR1. The dash-dotted, solid and dashed curves represent the corresponding linear fit to the data points.

In order to study the variation of magnetic field along the radial direction of the sunspots we made use of the broad-band images simultaneously recorded with the spectropolarimetric data. As the slit position on the image was known, the radial distance of each pixel on the slit was computed after identifying the centre

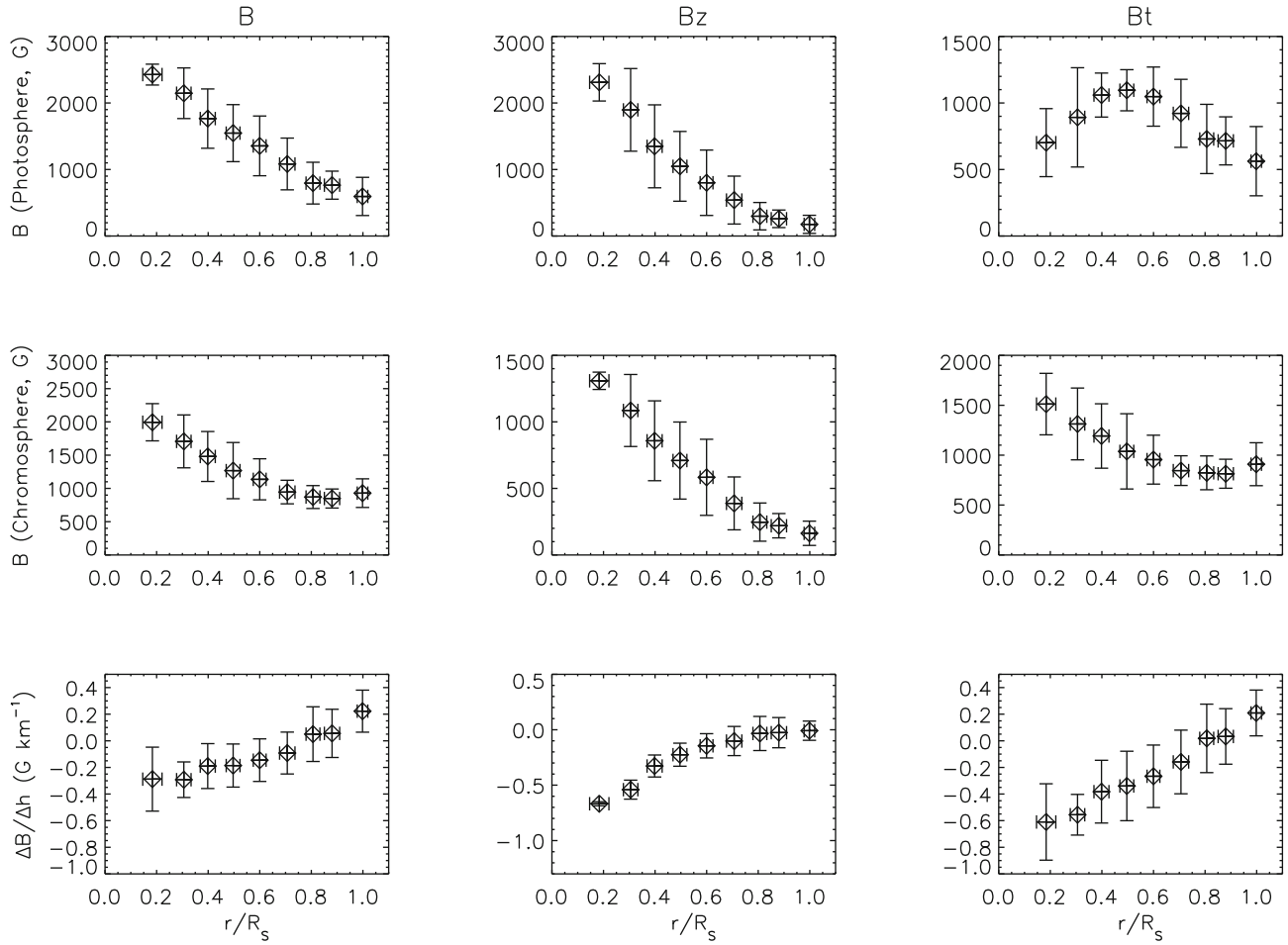

Figure 7. Same as Figure 6 but for AR2.

of the sunspot in the image, which corresponds to the darkest pixel of the sunspot, and manually identifying the edge of the sunspot (nothing but the sunspot radius R_s) in the corresponding radial direction. For estimating the LOS component of the magnetic field from the Hα line, Stokes I and V profiles were averaged over $1''$ along the slit and for estimating the transverse component, the Stokes profiles were averaged over $5''$. Accordingly photospheric magnetic field components derived from Fe I line were also averaged. The magnetic field parameters corresponding to a given radial distance were averaged and referred to as azimuthally averaged values (Borrero & Ichimoto 2011).

Vertical gradient of magnetic field is calculated as (Balthasar 2018)

$$\frac{\Delta B}{\Delta h} = \frac{B(\mathrm{H}\alpha) - B(\mathrm{Fe\ I})}{\Delta h}, \tag{3}$$

where Δh is the difference between the formation heights of Hα and Fe I lines, which is taken as 1500 km (Abdussamatov 1971). This definition of vertical gradient is consistent with Balthasar (2018). Negative value for the gradient implies that field is decreasing with height and positive value implies that field is increasing with height.

3. Results

The radial variation of azimuthally averaged magnetic field parameters is shown in Figure 6 for AR1 and in Figure 7 for AR2. The first and second row of panels show radial variation of magnetic field at the photosphere and chromosphere, respectively. The first, second and third column show the plots of B (total field strength), B_z (LOS component) and B_t (transverse component). The third row of panels show the corresponding vertical gradient $\Delta B/\Delta h$. The error bars are the dispersion values of respective parameter in the azimuthal direction. For both the spots B monotonically decreases with increase in radial distance r/R_s, where r is the radial distance from the centre of the sunspot and R_s is

the sunspot radius at the photosphere in a given radial direction. For AR1, B is close to 3000 G at the centre of the spot and reaches about 700 G at the edge of the sunspot. For AR2, B decreases from about 2500 G at the centre of the spot to about 500 G at the edge of the sunspot. B_z also shows a similar variation with its value close to B at the centre of the spot to almost zero at the edge of the spot. On the other hand, the B_t initially increases up to about $r/R_s \approx 0.55$ for AR1 and 0.5 for AR2 at which the B_z and B_t become comparable. After reaching the maximum, B_t component decreases monotonically towards the edge of the sunspot. These findings are consistent with the earlier study by Orozco Suarez *et al.* (2005), Borrero & Ichimoto (2011) and Joshi *et al.* (2017).

At the chromospheric heights, the B_z component decreases monotonically with the radial distance. Unlike in photosphere where B_t first increases and then decreases, at chromosphere its value decreases monotonically up to about $r/R_s = 0.6$ after which it reaches a constant value. The variation of B is similar to that of B_t as the dominant contribution to B is the transverse component. However, we would like to note here that because of the noisy Hα Stokes Q and U profiles, the estimation of transverse component is not reliable. Only at few locations they are above the noise level. Further, while it has been shown by Socas-Navarro and Uitenbroek (2004) that LOS component can be reliably derived by applying WFA to Stokes V profiles of Hα, application of WFA to Stokes Q and U profiles of Hα to derive the transverse component is yet to be validated.

The radial variation of $\Delta B/\Delta h$ is shown in the third row of Figures 6 and 7 above AR1 and AR2, respectively. For AR1 the gradient (absolute value) for B increases from a value of about -0.13 G km^{-1} close to centre of the sunspot to about -0.48 G km^{-1} at $r/R_s \approx 0.4$. After that the gradient starts to decrease and becomes positive with a value of 0.18 G km^{-1} close to the edge of the sunspot. A similar trend is observed for AR2 also but the maximum occurs at $r/R_s \approx -0.3$ with a value equal to ≈ -0.3 G km^{-1} and the gradient becomes positive already at $r/R_s \approx 0.8$. The maximum positive gradient occurs close to the edge of the sunspot with a value equal to ≈ 0.2 G km^{-1}. This behaviour is dictated predominantly by the transverse component of the magnetic field. On the other hand, the gradient in the LOS component shows monotonic decrease with increase in sunspot radius and asymptotically approach zero value close to the edge of the sunspot for both the sunspots. For AR1 the maximum LOS component gradient is -1.1 G km^{-1} close to the centre of the sunspot and becomes almost zero at the edge of the sunspot. For AR2, the maximum value is close to -0.67 G km^{-1} located close to $r/R_s = 0.2$ and becomes zero at the edge of the sunspot.

4. Conclusions

The global properties of the magnetic field derived from low spatial spectropolarimetric observations presented in the paper are consistent with the earlier findings that, at the photosphere the total and the LOS component of the magnetic field monotonically decreases with radial distance from the centre to the edge of the sunspot. On other hand, the transverse component initially increases with the radial distance from the centre of the sunspot to close to half the sunspot radius after which it decreases towards the edge of the sunspot. Close to half the sunspot radius of the LOS component of the magnetic field becomes comparable to that of transverse component. At the chromosphere, the LOS component of the magnetic field monotonically decreases with radial distance from the centre of the sunspot. Though we have presented about the radial variation of transverse component of the chromospheric magnetic field also in this paper, we did not give much emphasis on its properties because the values are not reliable due to poor SNR in the Stokes Q and U profiles of Hα. The vertical field gradient of ≈ -1 G km^{-1} derived from LOS components of photospheric and chromospheric magnetic field is also consistent with the earlier results. We have also reported about a, not so well known, line blend in the blue wing of Hα which is magnetically sensitive and found only in the cooler regions such as sunspot umbrae. The full line spectropolarimetric observations of Hα with improved SNR may provide a very useful diagnostic of chromospheric vector magnetic field.

Acknowledgements

We thank the observers Devendran and Hariharan for their help during observations.

References

Abdussamatov H. I. 1971, Solar Phys., 16, 384
Andretta V., Jones H. P. 1997, Astrophys. J., 489, 375
Auer L. H., House L. L., Heasley J. N. 1977, Solar Phys., 55, 47
Balasubramaniam K. S., Christopoulou E. B., Uitenbroek H. 2004, Astrophys. J., 606, 1233
Balasubramaniam K. S., Venkatakrishnan P., Bhattacharyya J. C. 1985, Solar Phys., 99, 333

Balthasar H. 2018, Solar Phys., 293, 120
Bappu M. K. V. 1967, Solar Phys., 1, 151
Bjørgen J. P., Leenaarts J., Rempel M., Cheung M. C. M., Danilovic S., de la Cruz Rodríguez J., Sukhorukov, A. V. 2019, Astron. Astrophys., 631, 33
Borrero J. M., Ichimoto K. 2011, Liv. Rev. Solar Phys., 8, 4
Casini R., Landi Degl'Innocenti E. 1994, Astron. Astrophys., 291, 668
Centeno R. 2018, Astrophys. J., 866, 89
Hanaoka Y. 2005, Pub. Astron. Soc. Japan, 57, 235
Jefferies J. T., Mickey D. L. 1991, Astrophys. J., 372, 694
Joshi J., Lagg A., Hirzberger J., Solanki S. K. 2017, Astron. Astrophys., 604, 98
Kerr G. S., Fletcher L., Russell A. e. J. B., Allred J. C. 2016, Astrophys. J., 827, 101
Kobanov N. I., Makarchik D. V., Sklyar A. A. 2003, Solar Phys., 217, 53
Kuridze D., Henriques V. M. J., Mathioudakis M., Rouppe van der Voort L., de la Cruz Rodríguez J., Carlsson M. 2018, Astrophys. J., 860, 10
Lagg A., Lites B., Harvey J., Gosain S., Centeno R. 2017, Space Sci. Rev., 210, 37
Landi Degl'Innocenti E., Landi Degl'Innocenti M. 1973, Solar Phys., 31, 299
Landi Degl'Innocenti E., Landolfi M. 2004, Polarization in Spectral Lines, Astrophysics and Space Library, Volume 307, Kluwer Academic Publishers, Dordrecht
Leenaarts J., Carlsson M., Rouppe van der Voort L. 2012, Astrophys. J., 749, 136
Lites B. W., Skumanich A. 1990, Astrophys. J., 348, 747
López Ariste A., Casini R., Paletou F. *et al*. 2005, Astrophys. J. Lett., 621, L145
Martínez González M. J., Bellot Rubio L. R. 2009, Astrophys. J., 700, 1391
Nagaraju K., Ramesh K. B., Sankarasubramanian K., Rangarajan K. E. 2007, Bull. Astro. Soc. India, 35, 307
Nagaraju K., Sankarasubramanian K., Rangarajan K. E. 2008a, Astrophys. J., 678, 531
Nagaraju K., Sankarasubramanian K., Rangarajan K. E., Ramesh K. B., Singh J., Devendran P., Hariharan 2008b, Bull. Astro. Soc. India, 36, 99
Orozco Suarez D., Lagg A., Solanki S. K. 2005, in Innes D. E., Lagg A., Solanki S. K., eds, Chromospheric and Coronal Magnetic Fields, ESA Special Publication 596, p. 59
Rutten R. J. 2007, in Heinzel P., Dorotovič I., Rutten R. J., eds, The Physics of Chromospheric Plasmas, ASP Conference Series, Volume 368, p. 27
Rutten R. J. 2008, in Matthews S. A., Davis J. M., Harra L. K., eds, First Results from *Hinode*, ASP Conference Series, Volume 397, p. 54
Sanchez Almeida J., Lites B. W. 1992, Astrophys. J., 398, 359
Sankarasubramanian K., Srinivasulu G., Ananth A. V., Venkatakrishnan P. 2000, J. Astrophys. Astron. 21, 241
Schlichenmaier R., Collados M. 2002, Astron. Astrophys., 381, 668
Skumanich A., Lites B. W. 1987, Astrophys. J., 322, 473
Socas-Navarro H. 2001, in Sigwarth M., ed., Advanced Solar Polarimetry—Theory, Observation and Instrumentation, PASP, 236, 487
Socas-Navarro H., Uitenbroek H. 2004, Astrophys. J. Lett., 603, L129
Uitenbroek H. 2006, in Leibacher J., Stein R. F., Uitenbroek H., eds, Solar MHD Theory and Observations: A High Spatial Resolution Perspective, PASP, 354, 313